Design of a compact active hip prosthesis with human-like range of motion and torque*

Louis Devillez[1], Benoît Herman[1] and Renaud Ronsse[1,2]

***Abstract*— Hip disarticulation and hemipelvectomy are the most severe forms of lower limb amputation, posing significant challenges to prosthetic solutions in terms of size, biomechanical functionality, and user compatibility. While active ankle and knee prostheses have made spectacular progresses recently in restoring a physiological gait, these advancements did not percolate yet to hip prosthesis design. This article introduces an innovative design of an active hip prosthesis displaying remote center of motion, and range of motion and torque compatible with the most ubiquitous locomotion tasks, i.e., walking and stand-to-sit-to-stand transitions. The designed structure incorporates a tilted double parallelogram mechanism, in order to optimize compactness and minimize internal constraints. The proposed hip prosthesis design features minimal encumbrance, with a horizontal size of 140 mm and a frontal width of 136 mm. Its range of motion spans from −30° to 90°, providing a comfortable sitting position with existing shell design. Remarkably, the mass of this hip joint is a mere 3.30 kg, excluding battery and power electronics.**

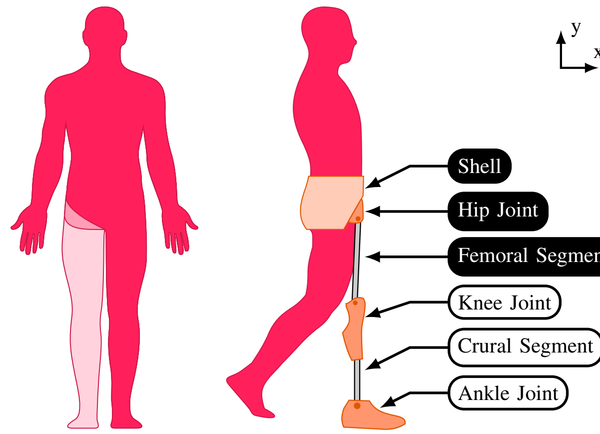

Fig. 1. Left: Schematic representation of the remaining body after hip disarticulation (medium red) and hemipelvectomy (red) in the frontal plane compared to a sound body (ligth red). Right: Schematic of a leg prosthesis with the main components of the hip module highlighted in black boxes and other modules annotated in white boxes.

I. INTRODUCTION

Hip Disarticulation and Hemipelvectomy (Fig 1, left) are the two most proximal amputation levels of the lower limb. Fortunately, these extremely mutilating interventions are not commonly performed. For example, they represent less than 0.4 % of all the lower limb amputations in Germany in 2019 [1]. The most frequent cause is to circumvent malignant bone sarcomas in the pelvis, like chondrosarcomas [2].

Hip prostheses have been developed since the 70's. The most frequently used device is called the "Canadian prosthesis" (Fig 1, right) and provides the replacement of the whole lower limb [3]. The main component of a typical Canadian prosthesis are a shell, fitting to the stump and transmitting bodyweight to the prosthesis; the hip joint itself, that is locked during the stance phase and loose otherwise; and the femoral segment connected to the prosthetic knee module.

Although they offer an efficient solution for disarticulated patients [4], these devices also induce several important complications due either to bone luxation or to the prosthesis itself (material fracture, component dislocation, etc.). Furthermore, despite being sophisticated and expensive, these prostheses do not sufficiently compensate for the lower limb loss up to the point of restoring normal biomechanical functions. In particular, their passive nature prevents them to replicate the mechanical energy production of a sound hip during ground level walking [5]. Consequently, they are frequently rejected for different reasons: awkwardness, intolerance of the socket, and excessive energy expenditure to ambulate, so that only about 33 % of the potential users have a daily use of their prosthesis [6].

Recent developments in the field promote the emergence of active solutions, i.e., prosthetic devices equipped with a power actuator. For instance, active ankles can reproduce the positive mechanical work of a sound joint during level-ground walking [5], up to normalizing the gait pattern of transtibial amputees, both regarding kinematics and metabolic cost [7], [8]. This has the potential to limit the onset of biomechanics related comorbidities such as osteoarthritis and low back pain [8]–[11].

However, these disruptive progresses regarding the restoration of motor functions for lower limb amputees focused on transfemoral and transtibial amputees, and only a few contributions targeted hip disarticulated patients. The low incidence of hip disarticulations in comparison to transfemoral and transtibial amputations [3] likely plays a role in this situation, on top of the intrinsic challenges associated with the mechanical replacement of the hip and its contribution for setting up locomotion rhythmicity for the whole leg [12]. This underscores the motivation for the design of a hip module in this study.

In the case of ankle and knee prostheses, there is a physical access to the joint center of motion. In contrast, for the hip, the center of motion is located in the pelvis, i.e., inside the shell, and is thus not physically accessible. To comply with the biomechanics of a sound hip, the center

*This work was supported by the Belgian F.R.S.-FNRS (Aspirant #40011487 awarded to LD)

[1]Institute of Mechanics, Materials and Civil Engineering and Louvain Bionics, UCLouvain, 1348 Louvain-la-Neuve, Belgium louis.devillez@uclouvain.be

[2]Institute of Neuroscience, UCLouvain, 1200 Brussels, Belgium

of motion of the prosthesis should coincide with its natural one. It is thus compulsory to implement a remote center of motion (RCM) in the mechanism. In order to enhance the potential usability of the prosthesis, we further assume that the shell should not be modified in order to be compatible both with a classical passive prosthesis and our proposed design. As direct consequence, the only attachment point lies in the front of a rigid plate embedded in the bottom of the shell. Furthermore we also assume that the prosthesis should allow a comfortable seated position to enhance usability. As consequence, the ideal device needs clearance below the shell.

A couple of active hip prostheses have been developped in the recent years; however none of them fullfiled all those requirements. In 2009, [13] proposed an active hip and knee prosthesis laterally mounted in order to align its rotation axis with the sound limb, and this required connection points below the shell. In 2018, *Össur hf* declared a patent for a powered hip prosthesis also with lateral mounting [14], necessitating shell modification, but this has not been transferred to the market yet. More recently, [15] introduced an active hip and knee prosthesis weighing nearly 10 kg and requiring shell modifications. Finally, an active hip prosthesis with a double parallelogram mechanism implementing a RCM has been unveiled in [16]. Yet, this design also requires fixation points below the shell. Later, the same design evolved to an active version requiring no modification of the shell [17], [18]. However, no evidence that this design allows the seated position has been provided.

The design reported in the present paper is inspired by [16]–[18], yet with a critical change in the morphology of the double parallelogram mechanism, such that the range of motion and torque is compatible with walking, standing, and sitting. The paper is structured as follows. Section II presents the problem statement, i.e., establishes the specifications inherent to the intended design. Section III highlights the specific morphology of the modified double parallelogram and its dimensioning. Section IV focuses on the integration of the actuator in the prosthesis. A detailed CAD design of the prototype is presented in Section V. Section VI describes the study about mass budget for further integration of knee and ankle modules. The paper ends with a discussion and conclusion.

II. PROBLEM STATEMENT

Walking is the most fundamental locomotion task. Therefore, the first step towards the replacement of biomechanical functions is to restore the ability to walk to someone with hip disarticulation. Emulating walking kinematics and kinetics is the main driver of the design of the prosthesis. However, before starting a walk, people often need to stand up from a chair. The capacity to support this Stand-to-Sit-to-Stand (StSiSt) transition is thus also central in our design, in order to provide the largest possible support during these transition tasks. Figure 2 represents the biological hip torque, normalized to the user's bodyweight, as a function of angular position during both tasks (walking and StSiSt). Walking

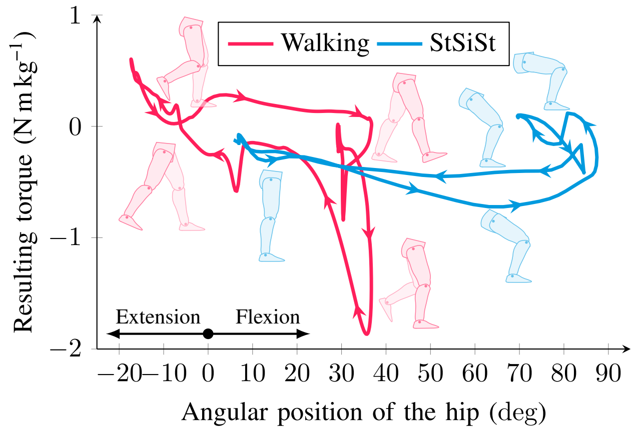

Fig. 2. Normalized torque vs angle relationship of a sound human hip during a walking gait cycle and a Stand-to-Sit-to-Stand transition. Key leg positions are illustrated.

data are directly taken from [19], while for StSiSt, the angular profile is taken from [20] and the torque profile has been computed by inverse dynamics using our home-made multibody software *Robotran* [21] in order to account for similar masses and segment lengths as in [19]. The required range of motion of the hip lies thus from $-20°$ in extension up to $90°$ in flexion. The absolute torque rises up to $1.9\,\mathrm{N\,m\,kg^{-1}}$ at the beginning of the single support phase during walking.

Moreover this range of motion and torque has to be delivered through a RCM mechanism, since the location of the biological hip center of motion is not accessible. A double parallelogram mechanism is a classical way to implement a fixed RCM. An implementation of this mechanism embodied as a hip prosthesis is provided in Fig 3. Point l, capturing the attachment point of the knee module, has to rotate around point o, capturing the hip natural center of motion. A classical straight double parallelogram (in green, and similar to the one developed in [16]–[18]) can achieve this kinematics via a single attachment point a to the shell. The first parallelogram $BCDE$ keeps ED parallel to BC. Point F extends segment ED such that the length EF is equal to the distance between o and B. Considering the virtual parallelogram $oBEF$, one can thus see that moving the first parallelogram makes F rotating along a circle of center o and radius BE. The second parallelogram $EFGH$ guarantees that the femoral segment always stays oriented towards the remote center o. Point H lies in the prolongation of segment BE. Similarly as for F, point G rotates effectively around the center o. FG can thus be extended until point l where the knee module is attached. The lengths of the different segments have to be selected in order to avoid collision with the shell in the desired motion range.

The main limitation of this mechanism is that it protrudes largely away from the volume of a biological thigh. A key reason explaining this encumbrance is the location of the main fixation point a, that must be near the top of the rigid plate. Indeed, the absolute orientation of this segment — defined as the angle β, see Fig 3 — cannot be decreased too much if the device has to reach an angular position θ of about

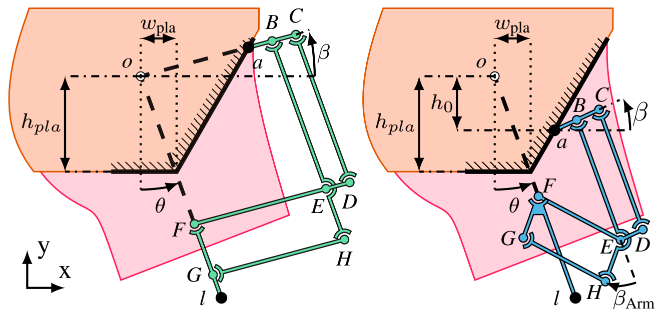

Fig. 3. Kinematic diagram of the straight (green) and of the tilted (blue) double parallelogram mechanism attached to the rigid plate (hatched zone) of the shell (orange). Uppercase letters represent joints and lowercase letters represent attachment points for either the shell or the knee module.

90° when sitting down. For $\beta \leq 0°$, the mechanism would indeed reach a singular configuration over its movement range. This must be avoided since no torque could be delivered through the prosthesis in such a singular configuration. For the same reason, the more the parallelograms are folded, the more the internal stresses rise in their joints. Taking $\beta > 0°$ and large enough reduces this constraint that will directly impact the structure dimensioning. Similarly, reducing the distance *BC* degenerates the parallelogram in a way that internal stresses will rise; and reducing the distance *aB* is limited by the physical space required for the connection and the assembly.

III. TILDED DOUBLE PARALLELOGRAM

A. Conceptual principle

A modified version of the double parallelogram mechanism is proposed with a tilted double parallelogram, also depicted in Fig 3 (blue). It starts by considering a lower attachment point a as a hard constraint, in order to decrease the mechanism encumbrance. The vertical distance between the center of motion o and this attachment point a is defined by the parameter h_0. Importantly, the virtual shape defined by *oBEF* must keep the shape of a parallelogram, otherwise *F* will not rotate about o. This is achieved by tilting the second parallelogram in such a way that *EF* is parallel (and of equal length) to *oB*. The offset angle β_{arm} between *BE* and *EH* is a free parameter that must be tuned such that the parallelogram *EFGH* never reaches a singular configuration across its movement range. As such, *F*, *l*, and *o* belong to the same line, such that the kinematics of the attachment point of the knee module *l* is similar to the straight implementation previously presented.

B. Topological optimization

By comparing both mechanisms, it clearly appears that the tilted double parallelogram is more compact than the straight version for a given angle β and a given length l_{BC} (distance between points *B* and *C*). In order to make this comparison more quantitative, the morphology of both mechanisms can be optimized with the objectives to minimize (i) their horizontal size at rest while standing, i.e.,

$$O_{size} = ||oa||_x + l_{aC}\cos\beta \tag{1}$$

and (ii) the maximum shaft diameter of the double parallelogram joints. This shaft diameter directly depends on the corresponding internal forces being generated by action-reaction through the different segments. In the case of the tilted double parallelogram, all these internal forces are represented in a series of free body diagrams in Fig 4 (red), together with the actuation torque (green) required to maintain the mechanism in steady-state, and the external force and torque applied at the fixation point a and at the connection to the knee module l (blue). Their magnitude and orientation directly depend on the geometrical parameters of the mechanism, on the flexion angle θ, and on the external forces and torques applied to the prosthesis. A similar drawing can be made for the straight double parallelogram.

These external force and torque have been derived from inverse dynamics simulations. Next, computation of internal forces has been achieved with *Robotran* for both the walking and the StSiSt tasks. By following the methodology from [22], each joint shaft can be dimensioned, with the following specifications: lifetime of 5 year, 4000 steps and 71 StSiSt transitions per day [23]. Each shaft minimum diameter can then be computed as,

$$d_{\min} = \sqrt[3]{\frac{32LF_a}{\pi\sigma_{ea}}S_F} \tag{2}$$

with σ_{ea} defined as

$$\sigma_{ea} = \frac{\frac{F_a}{F_m}}{\frac{F_a}{F_m} + \frac{S_n}{S_u}} S_n \tag{3}$$

F_m represents the mean force during the cycle and F_a the amplitude of its variation; L is the length of the shaft; S_u is the ultimate tensile strength of the material; and S_n is its endurance limit which depends on other factors such as the lifetime, the temperature and the desired reliability.

The optimized parameters of the mechanism are the angle β and the length l_{BC}. Values of all the parameters are given in Table I. The optimization was done with the module NSGA-II of *Optimeed* [24]. Results are given in Fig 5. It clearly appears that the tilted double parallelogram is more compact: for a given shaft diameter, it is about 60 mm shorter.

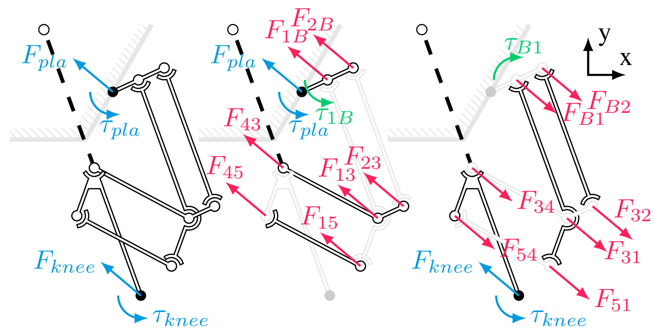

Fig. 4. Left: Free body diagram of the whole tilted double parallelogram. Center and right: Free body diagram of each internal segment of the mechanism. According to Newton's third law, $F_{ij} = -F_{ji}$. Virtual actuation torque is represented in green, while external (resp. internal) efforts are represented in blue (resp. red).

TABLE I

PARAMETERS USED IN THE OPTIMIZATION OF THE DIFFERENT IMPLEMENTATIONS OF THE DOUBLE PARALLELOGRAM

Fixed Parameters			
Name	**Value**	**Name**	**Value**
w_{pla}	37.5 mm	h_{pla}	97.1 mm
h_0	72 mm	β_{arm}	55°
l_{aB}	25 mm	l_{CD}	160 mm
l_{EH}	35 mm	l_{ol}	430 mm
S_F	2	S_U	638 MPa
$S_{n,\text{StSiSt}}$	227 MPa	$S_{n,\text{walking}}$	191 MPa
L	10 mm		
Parameters being optimized			
Name	**Range**	**Name**	**Range**
β	[1°, 25°]	l_{BC}	[10 mm, 50 mm]
Extra parameters being optimized with the actuated mechanism			
Name	**Range**	**Name**	**Range**
γ	[0°, 20°]	l_{DK}	[20 mm, 80 mm]
r	[1.2, 3]	l_s	[1 mm, 4 mm]

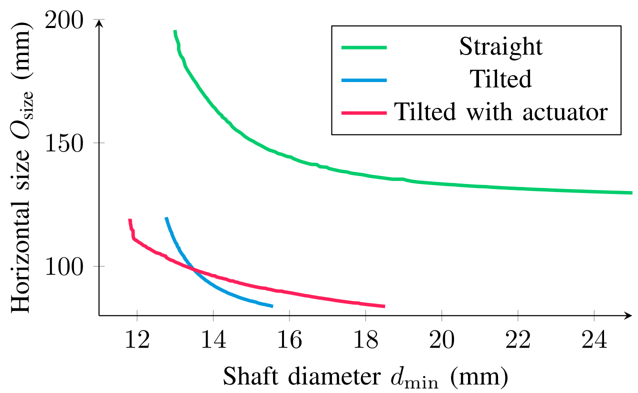

Fig. 5. Pareto front capturing the minimum largest shaft diameter of the joints and the smallest horizontal size from the optimization of the straight, tilted, and tilted with actuator double parallelogram.

IV. DESIGN OF THE ACTUATOR

In this section, a motor and transmission to actuate the kinematic structure defined in the previous section is designed. The prosthesis needs to follow the kinematics and the torque reported in Section II. Integrating a gearbox in the volume of the prosthesis is not considered as a favorable option since it would need to deliver up to 150 N m (for an 80 kg user) and would significantly impact the device mass.

As an alternative, we decided to implement a transmission with a powerscrew directly actuating one of the device segments (Fig 6, top left). A motor is attached to the part *DEF* and is coupled to the powerscrew via a belt. This powerscrew translates (x) a carriage which is connected to the bar *CD* with two extra joints, denoted *I* and *K*, and a connecting rod. Moving the carriage will change the length *ID* of the triangle *IDK* and therefore its angles, and eventually the angle of the prosthesis θ.

The geometrical parameters of this transmission are l_{DK}, r (the ratio between l_{KI} and l_{DK}), γ (the angle defined between *DE* and the axis of the carriage *DI*) and l_s (the lead of the powerscrew). The force exerted by the powerscrew and the position of the carriage can be expressed as,

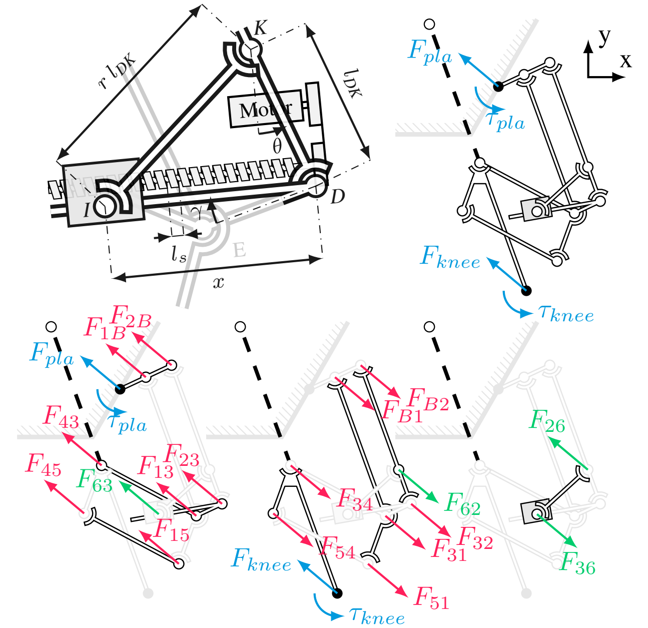

Fig. 6. Top left: Schematic of the crank handle transmission embedded in the tilted double parallelogram with its four geometric parameters: l_{DK}, r, γ and l_s. Top right: Free body diagram of the tilted double parallelogram embedding this actuator. Bottom: Free body diagram of each internal segment of the mechanism. Actuation forces are represented in green, while external (resp. internal) efforts are represented in blue (resp. red).

$$F = \frac{1}{ar}\frac{\cos(\theta-\gamma)}{\tan(\varphi)\cos(\varphi-\theta+\gamma)}(\tau_{knee} + l_{ol}\times F_{knee}) \quad (4)$$

$$x = a\sin(\theta-\gamma) + ar\cos(\varphi) \quad (5)$$

with $\varphi = \arcsin\left(\frac{\cos(\theta-\gamma)}{r}\right)$, while the corresponding motor torque and velocity for this non-backdriveable transmission are:

$$\omega = \frac{2\pi}{l}\dot{x} \quad (6)$$

$$\tau = \frac{Fl}{2\pi\eta} + \frac{I\dot{\omega}}{\eta} \quad (7)$$

I represents the inertia of both the motor and transmission, while η denotes the efficiency of the transmission. The ideal motor would be the lightest one satisfying two conditions: both the maximum velocity and the RMS torque of the motor during a task should be smaller than nominal values reported in the datasheet.

One of the lightest motors being compatible with these requirements is the *EC 60 flat 200W 48V* (Maxon, Sachseln, Switzerland). Adding this actuator to the mechanism also changes its free body diagram (Fig 6) and thus the Pareto front capturing the minimal size and shaft diameter (Fig 5, red). The parameters for the double parallelogram were consistent with those reported in Section III, while the supplementary parameters to be optimized are also documented in Table I. With the incorporation of the actuator, the shaft size can be reduced to 12 mm, a standard dimension for various mechanical components. This establishes the value for all optimized parameters as: β = 20.5°, γ = 15°, l_{BC} = 42 mm, l_{DK} = 47 mm, r = 1.43 and l_s = 3 mm. The selected powerscrew is the *MTSBRV14* (Misumi, Schaumburg, USA).

Eq. (4) captures one advantage of this transmission which is its non-linearity: this allows to have a high transmission ratio and therefore high torque when it is the most needed, i.e., at the beginning of the single support phase, see Fig 7.

V. PROTOTYPE

After having determined the main parameters of the device structure and actuator, this section overviews the first version of the detailed design, as depicted in Fig 8.

The structure is essentially composed of flat aluminium rods (AW7075-T651), shaped to prevent any undesired collision and to achieve the most compact configuration in a seated position. The kinematic structure is replicated on both the left and right sides with connecting parts to enhance rigidity in the frontal plane. This duplication allows the natural placement of the motor (9), powerscrew (7) and carriage (8) between these mirrored parallelograms. The base (3) connecting the prosthesis to the shell can also be placed in this central space. The pyramidal adapter (4) provides adaptability in thigh length by allowing the selection of different femoral tube lengths to connect to the knee module. The part *IDEF* is also divided into 2 physical components for facilitating the fabrication and to improve the compacity with a fully foldable mechanism.

The carriage incorporates four linear ball bearings for guidance on two parallel shafts (6) running alongside to the powerscrew. The motor is connected to the powerscrew through a pair of pulleys (10), safeguarded by a cover. The prosthesis range of motion spans from −30° up to 90°, and is mechanically constrained by the carriage stroke. End-of-motion switches (5) are placed to detect these events. The motor includes a rotary encoder to measure the prosthesis angle relative to the shell, and an absolute encoder can be positioned at joint B for closed-loop control of the prosthesis and/or data acquisition. All joints consist of 12 mm steel (C45E) shafts and ball bearings (joints D, F, G) or plain bearings (joints B, C, E, H, K, I).

Fig 8 further provides an idealized representation of the shell (1) and its regular attachment point (2). Using our CAD software, the transmission is estimated to weight 1.7 kg and the double kinematic structure (excluding the base) is estimated to weight 1.09 kg. This prototype has been fabricated and assembled (Fig 9) and its measured mass is 3.30 kg, excluding the mass of a battery and of the drive electronics. This is of course more than the 0.88 kg of a typical passive module [25].

VI. TOWARDS COMPATIBLE KNEE AND ANKLE MODULES

A challenge for current active knee prostheses is their compatibility with ankle modules. During the swing phase, the prosthetic knee has to accelerate and decelerate both the mass of its own moving parts, and the remote ankle module. Having a too heavy ankle prosthesis could thus limit the knee and disrupt its proper functioning. For the hip, a similar problem exists, but this time with the requirements that the hip should be powerful enough to accelerate/decelerate both the knee and the ankle during the swing phase. In order to evaluate the compatibility of our designed prosthesis

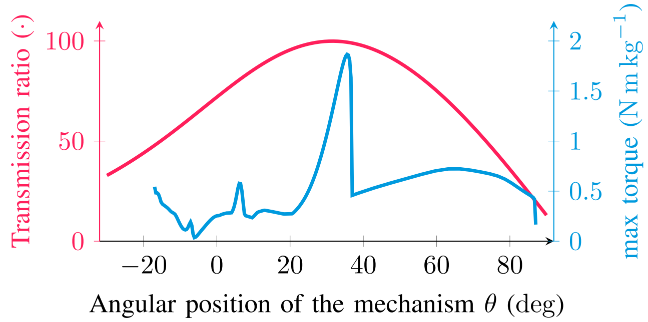

Fig. 7. Transmission ratio (red) of the actuated mechanism and maximum required normalized torque (blue) as a function of its angular position.

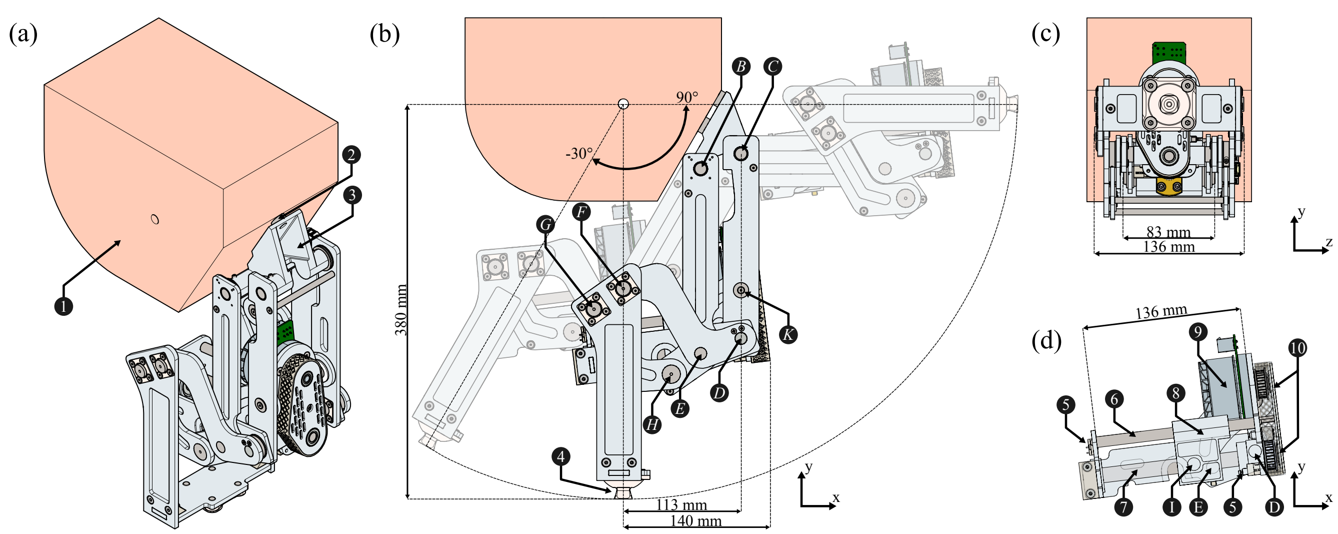

Fig. 8. Complete CAD design of the prosthesis; (a) corner view in the standing position, (b) sagittal view in standing position with both extrema being semi-transparent, (c) frontal view of the sitting position, (d) sagittal view of the transmission with the front bar being transparent. Numbers represent parts of the prosthesis: (1) simplified shell representation, (2) rigid plate attachment point, (3) base, (4) pyramidal adapter, (5) micro-switch, (6) guiding rails, (7) powerscrew, (8) carriage, (9) motor, (10) pulleys. Uppercase letters represent joints, with the same nomenclature as in Figs 3 and 6.

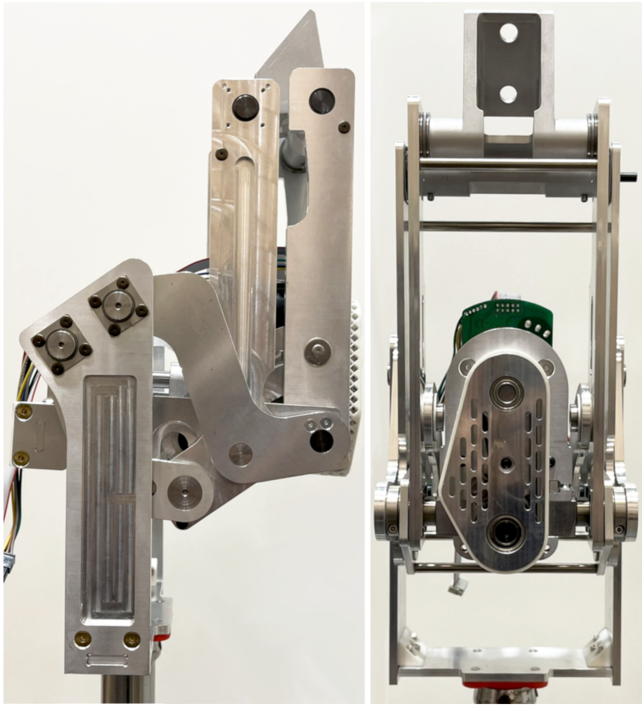

Fig. 9. Views of the prototype. Left: sagittal view. Right: Frontal view.

with other devices, an artificial leg (Fig 10, left) has been simulated to follow the same kinematics as the one used for our design and with potential knee and ankle modules combined as a whole prosthetic leg. The length of each segment (l_h: 430 mm, l_k: 430 mm and l_a: 180 mm) are taken from [26] considering a male subject and the center of mass of each prosthetic module is placed at their corresponding joint except for our hip module where it is placed according to the CAD (200 mm below the RCM). Simulations did not consider the inherent inertia of each module.

Required hip torque to move this artificial leg is computed using inverse dynamics, again with *Robotran*. We ran this simulation considering a set of knee and ankle masses in the following range: from 0 to 2.6 kg for the ankle, and from 0 to 6 kg for the knee. The exploration of this space leads to the results given in Fig 10, right. All combinations inside the dashed line are compatible with our hip module, since they require a RMS actuation torque during the swing phase below the one that the motor can deliver through our module.

Finally, we assessed the viability of our hip module with existing knee and ankle active devices. In particular, integrated ankle and knee prototypes such as the Open Source Leg [27], the Utah Bionic Leg [28] and the CYBERLEG Beta prosthesis [29], are all compatible with our design. We also validated compatibility with combinations taken from the catalogue of the main manufacturers: the Empower (active ankle module) with the Genium X3 (recommended passive knee) from *Ottobock*, and the Power knee (active knee module) with the Pro-Flex XC-Torsion (recommended passive ankle) from *Össur*. The combination from *Össur* lies inside the compatibility region, while the ankle module from *Ottobock* is too heavy when associated with their knee to be compatible with our hip module.

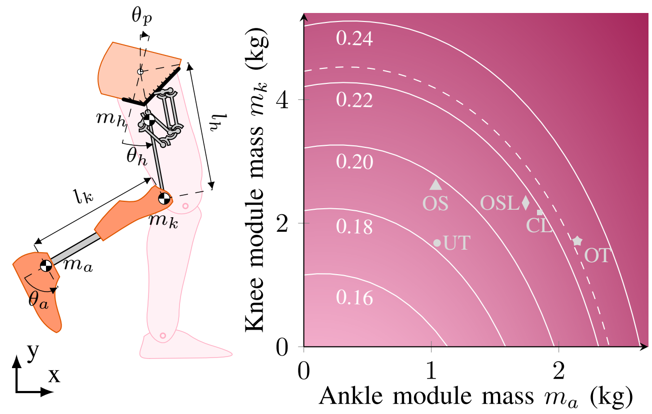

Fig. 10. Left: Geometrical parameters of the artificial leg. The subscripts p, h, k and a correspond respectively to the pelvis, hip, knee and ankle. Right: RMS torque value during the swing phase of the walking gait for different masses of ankle and knee. The dashed line represent the current limit of the prosthesis. The markers depict existing prostheses: Open Source Leg (OSL) [27], Utah Bionic Leg (UT) [28], CYBERLEG Beta prosthesis (CL) [29], Power Knee and Pro-Flex XC-Torsion from *Össur* (OS), Genium X3 and Empower from *Ottobock* (OT).

VII. DISCUSSION & PERSPECTIVES

The proposed hip module based on the tilted double parallelogram brings unique features as compared to state-of-the-art solutions.

A. Compactness

In comparison to the hip module presented in [18], the most recent and advanced hip module to date and that relies on a straight double parallelogram mechanism, our proposed design displays better compactness. Specifically, the size along the x-axis in the sagittal plane of the kinematic structure of [18] is reported to be 142 mm, whereas ours is notably smaller, i.e., 113 mm. Even the size of the furthest point on our prototype (bottom of the pulley cover in a standing position) is 140 mm. These sizes depend on the parameters of the rigid plate (h_pla, w_pla), which were not provided in [18]. The length (y-axis) of the module of [18] is 415 mm, while ours is 380 mm. Although the width (z-axis) of the hip module in the frontal plane of [18] has not been found in the corresponding publications, the width of our design is 136 mm, and thus safely meets their requirement of 146 mm.

B. Seated position and shell modification

The study presented in [18] did not provide evidence of the possibility to reach a seated position or to perform StSiSt transitions with their design. However, it is noteworthy that their module does not require modification of the shell which should allow reaching a seated position. More critically, other designs like those reported in [13]–[16] involved modifications to the shell, in particular through the addition of other connection points at the bottom of it, potentially impacting the ability to sit comfortably.

In our design, careful consideration was given to comply with the seated position and to guarantee clearance under the shell. By maintaining the integrity of the shell, we aim at enhancing the potential usability of our module by people currently using state-of-art devices.

C. Future developments

A functional prototype has been assembled recently, validating the RCM implementation and the angular range of motion. The primary objective of this prototype is to provide a first functional validation of the specifications. In particular, rig-based experiments will be conducted to assess both the kinematic and torque ranges, allowing for a comparison with the desired trajectories. The following step will be to design a closed-loop controller for walking and StSiSt transitions. Finally, design updates will focus on the integration of a battery pack and control electronics.

VIII. CONCLUSION

This paper introduces a tilted double parallelogram mechanism and transmission for an active yet compact hip prosthesis. Tilting of the most distal parallelogram unlocks critical design constraints, enabling a decrease in the horizontal size and the internal forces inside the mechanism, as compared to a standard straight double parallelogram. Providing actuation through a powerscrew, instead of through a direct rotational actuation and a gearbox, not only further decreases internal forces but provides a high transmission ratio when needed. These design choices have successfully resulted in a light (measured weight of 3.30 kg) and compact hip module (140 mm x 380 mm x 136 mm) with a range of motion from −30° to 90° and with no need of modifying standard shell. While experimental validation of the prototype is pending, preliminary studies on its integrability with knee and ankle modules show promising prospects.

REFERENCES

[1] N. Walter, V. Alt, and M. Rupp, "Lower Limb Amputation Rates in Germany," *Medicina*, vol. 58, no. 1, p. 101, Jan. 2022. DOI:10/gtbrb4

[2] T. Ozaki, A. Hillmann, N. Lindner, S. Blasius, and W. Winkelmann, "Chondrosarcoma of the pelvis," *Clinical Orthopaedics and Related Research*, vol. 337, pp. 226–239, 1997. DOI:10/d64hs9

[3] G. Stark, "Overview of Hip Disarticulation Prostheses," *JPO: Journal of Prosthetics and Orthotics*, vol. 13, no. 2, pp. 50–53, June 2001. DOI:10/cgsrgh

[4] A. J. Aboulafia, R. Buch, J. Mathews, W. Li, and M. M. Malawer, "Reconstruction using the saddle prosthesis following excision of primary and metastatic periacetabular tumors," *Clinical orthopaedics and related research*, no. 314, pp. 203–213, May 1995.

[5] D. A. Winter, *Biomechanics and Motor Control of Human Movement*. John Wiley & Sons, Oct. 2009.

[6] A. Fernàndez and J. Formigo, "Are Canadian Prostheses Used? A Long-Term Experience," *Prosthetics and Orthotics International*, vol. 29, no. 2, pp. 177–181, Aug. 2005. DOI:10/dgbjd4

[7] M. F. Eilenberg, H. Geyer, and H. Herr, "Control of a Powered Ankle–Foot Prosthesis Based on a Neuromuscular Model," *IEEE Transactions on Neural Systems and Rehabilitation Engineering*, vol. 18, no. 2, pp. 164–173, Apr. 2010. DOI:10/dtcw55

[8] H. M. Herr and A. M. Grabowski, "Bionic ankle–foot prosthesis normalizes walking gait for persons with leg amputation," *Proceedings of the Royal Society B: Biological Sciences*, vol. 279, no. 1728, pp. 457–464, Feb. 2012. DOI:10/d3hjmw

[9] D. C. Morgenroth, A. D. Segal, K. E. Zelik, J. M. Czerniecki, G. K. Klute, P. G. Adamczyk, M. S. Orendurff, M. E. Hahn, S. H. Collins, and A. D. Kuo, "The effect of prosthetic foot push-off on mechanical loading associated with knee osteoarthritis in lower extremity amputees," *Gait & Posture*, vol. 34, no. 4, pp. 502–507, Oct. 2011. DOI:10/dhc9r7

[10] B. E. Lawson, J. Mitchell, D. Truex, A. Shultz, E. Ledoux, and M. Goldfarb, "A Robotic Leg Prosthesis: Design, Control, and Implementation," *IEEE Robotics Automation Magazine*, vol. 21, no. 4, pp. 70–81, Dec. 2014. DOI:10/gpd984

[11] P. Cherelle, V. Grosu, M. Cestari, B. Vanderborght, and D. Lefeber, "The AMP-Foot 3, new generation propulsive prosthetic feet with explosive motion characteristics: Design and validation," *BioMedical Engineering OnLine*, vol. 15, no. 3, p. 145, Dec. 2016. DOI:10/gs8tww

[12] F. Dzeladini, J. van den Kieboorm, and A. Ijspeert, "The contribution of a central pattern generator in a reflex-based neuromuscular model," *Frontiers in Human Neuroscience*, vol. 8, p. 371, 2014. DOI:10/gk5dpc

[13] N. Hata, T. Kubo, and T. Inoue, "Development of a Powered Hip Disarticulation Prosthesis with Swing Phase Controller," *Transactions of the Japan Society of Mechanical Engineers Series C*, vol. 75, no. 750, pp. 404–412, 2009. DOI:10/gs8tw2

[14] D. Langlois, A. V. Clausen, and Á. Einarsson, "Powered prosthetic hip joint," US Patent US9 895 240B2, Feb., 2018. https://patents.google.com/patent/US9895240B2/en

[15] Y. Ueyama, T. Kubo, and M. Shibata, "Robotic hip-disarticulation prosthesis: Evaluation of prosthetic gaits in a non-amputee individual," *Advanced Robotics*, vol. 34, no. 1, pp. 37–44, Jan. 2020. DOI:10/gs8tw5

[16] Xinwei Li, Z. Deng, Q. Meng, S. Bai, W. Chen, and H. Yu, "Design and optimization of a hip disarticulation prosthesis using the remote center of motion mechanism," *Technology and Health Care*, vol. 29, no. 2, pp. 269–281, Jan. 2021. DOI:10/gs8tw6

[17] M. Fan, Y. Chen, B. He, Q. Meng, and H. Yu, "Study on Adaptive Adjustment of Variable Joint Stiffness for a Semi-active Hip Prosthesis," in *Intelligent Robotics and Applications*, ser. Lecture Notes in Computer Science, H. Liu, Z. Yin, L. Liu, L. Jiang, G. Gu, X. Wu, and W. Ren, Eds. Cham: Springer International Publishing, 2022, pp. 13–23.

[18] S. Luo, X. Shu, H. Zhu, and H. Yu, "Design and optimization of a new integrated hip and knee prosthesis structure," *Artificial Organs*, vol. 2023, no. 00, July 2023. DOI:10/gs8tw4

[19] H. Geyer and H. Herr, "A Muscle-Reflex Model That Encodes Principles of Legged Mechanics Produces Human Walking Dynamics and Muscle Activities," *IEEE Transactions on Neural Systems and Rehabilitation Engineering*, vol. 18, no. 3, pp. 263–273, June 2010. DOI:10/cs6tf4

[20] M. Błażkiewicz, I. Wiszomirska, and A. Wit, "A new method of determination of phases and symmetry in stand-to-sit-to-stand movement," *International Journal of Occupational Medicine and Environmental Health*, vol. 27, no. 4, pp. 660–671, Aug. 2014. DOI:10/gs8twv

[21] N. Docquier, A. Poncelet, and P. Fisette, "ROBOTRAN: A powerful symbolic gnerator of multibody models," *Mechanical Sciences*, vol. 4, no. 1, pp. 199–219, May 2013. DOI:10/gs8twx

[22] R. Juvinall and K. Marshek, *Fundamentals of Machine Component Design, 5th Edition*. Wiley, 2011.

[23] M. Puliti, F. Tessari, R. Galluzzi, S. Traverso, A. Tonoli, L. De Michieli, and M. Laffranchi, "A Hybrid Swing-Assistive Electro-Hydrostatic Bionic Knee Design," in *2022 9th IEEE RAS/EMBS International Conference for Biomedical Robotics and Biomechatronics (BioRob)*, Aug. 2022, pp. 01–07.

[24] C. De Gréef, "Optimeed," Louvain-la-Neuve, Belgium, Oct. 2023. https://git.immc.ucl.ac.be/chdegreef/optimeed

[25] "Modular Hip Joint Free Mot. Titan." https://shop.ottobock.ca/en/Prosthetics/Lower-Limb-Prosthetics/Hips/Modular-Hip-Joint-Free-Mot-Titan/p/7E7

[26] R. Dumas, L. Chèze, and J. P. Verriest, "Adjustments to McConville et al. and Young et al. body segment inertial parameters," *Journal of Biomechanics*, vol. 40, no. 3, pp. 543–553, Jan. 2007. DOI:10/dgqgfz

[27] A. F. Azocar, L. M. Mooney, J.-F. Duval, A. M. Simon, L. J. Hargrove, and E. J. Rouse, "Design and clinical implementation of an open-source bionic leg," *Nature Biomedical Engineering*, vol. 4, no. 10, pp. 941–953, Oct. 2020. DOI:10/gs8twt

[28] M. Tran, L. Gabert, S. Hood, and T. Lenzi, "A lightweight robotic leg prosthesis replicating the biomechanics of the knee, ankle, and toe joint," *Science Robotics*, vol. 7, no. 72, p. eabo3996, Nov. 2022. DOI:10/gq956h

[29] L. Flynn, J. Geeroms, R. Jimenez-Fabian, S. Heins, B. Vanderborght, M. Munih, R. Molino Lova, N. Vitiello, and D. Lefeber, "The Challenges and Achievements of Experimental Implementation of an Active Transfemoral Prosthesis Based on Biological Quasi-Stiffness: The CYBERLEGs Beta-Prosthesis," *Frontiers in Neurorobotics*, vol. 12, 2018. DOI:10/gfrpqk